Black Sea rivers capture significant change in catchment-wide mean annual temperature and soil pH during the Miocene-to-Pliocene transition

Iuliana Vasiliev[a,b,*], Gert-Jan Reichart[c,d], Wout Krijgsman[e], Andreas Mulch[a,f]

[a] Senckenberg Biodiversity and Climate Research Centre BiK-F, Senckenberganlage 25, D-60325 Frankfurt am Main, Germany
[b] Faculty of Geology and Geophysics, Bucharest University, Bălcescu Bd., Bucharest 010041, Romania
[c] Royal Netherlands Institute of Sea Research, P.O. Box 59, 1790 AB Den Burg, Texel, the Netherlands
[d] Department of Earth Sciences, Utrecht University, Budapestlaan 4, 3584 CD Utrecht, the Netherlands
[e] Paleomagnetic Laboratory 'Fort Hoofddijk', Department of Earth Sciences, Utrecht University, Budapestlaan 17, 3584 CD Utrecht, the Netherlands
[f] Institute for Geosciences, Goethe University Frankfurt, Frankfurt am Main 60438, Germany

ARTICLE INFO

ABSTRACT

The Neogene sedimentary successions of the Black Sea basin are ideal to study ancient paleoclimatic and hydrological changes in the Eurasian continental interior. Previous investigations revealed several phases of strongly enhanced evaporitic and dry conditions in the late Miocene. Here, we present the first reconstructed mean annual air temperature (MAAT) and soil pH data, combined with compound specific hydrogen isotopic (δD) records for the late Miocene to early Pliocene Black Sea basin, based on the analyses of biomarkers. Our MAAT, pH and δD data indicate that in the latest Tortonian (~8–7 Ma) mean annual air temperatures were approximately 5° higher than today, and that dry and warm climatic conditions prevailed. The early Messinian (7–6 Ma) is marked by a gradual change towards more humid, but still warm, conditions. The MAAT record shows a sharp decrease from 16 to 8 °C during the late Messinian (6.2–5.8 Ma) coinciding with a change towards extremely dry conditions. This cold and dry interval correlates to the time span marked by the late Miocene cooling of the northern hemisphere, and may also reflect a sea level change, restricting the Azov/Taman basin from the Black Sea. The calculated soil pH values in the range 7.1 to 7.7 are indicative for alkaline soils, such of those in the northern Eurasian hinterland, indicating a dominant northern Black Sea riverine source for the soil biomarkers. Finally, the Pliocene is marked by warmer conditions and lower soil pH, indicating a revival of the climatic conditions that characterized the Black Sea area during the late Messinian.

1. Introduction

Due to the protracted effects of tectonics and climate the Black Sea basin represents an ideal target to study the continental response to ancient changes in connectivity to marine realm and environmental conditions. During the Miocene, the stepwise restriction of the Black Sea basin (i.e. Eastern Paratethys, Fig. 1) from the global oceans resulted in environments marked by highly varying salinities, from marine to brackish and fresh water conditions (e.g. Popov et al., 2006; Vasiliev et al., 2015; Palcu et al., 2017) and the development of highly endemic biota (e.g. Popov et al., 2016; Stoica et al., 2016). Recently, compound-specific hydrogen isotope (δD) data from excellently preserved alkenones and *n*-alkanes, derived from haptophyte algae and plant waxes, respectively, were used to reconstruct past changes in the hydrology of the Black Sea basin (Vasiliev et al., 2013). Based on these data, two phases of severe drought were identified: 1) the latest Tortonian-earliest Messinian (between ~8 and 7 Ma) (Vasiliev et al., 2015) and 2) the interval between ~5.8–5.6 Ma when the Black Sea became restricted and temporally isolated from the Mediterranean during the first phase of the so-called Messinian Salinity Crisis (Vasiliev et al., 2013, 2015).

To frame these hydrological changes governed by the intermittent Black Sea-Mediterranean connectivity within a context of continental climate change, we present mean annual air temperature data (MAAT) of the northern continental basin margin (Taman Peninsula, Russia) based on the relative distribution of branched glycerol dialkyl glycerol tetraether (brGDGT) lipids primarily derived from soil bacteria (Weijers et al., 2007a7a). The brGDGT lipid record further serves for the reconstruction of soil pH within the catchment of the rivers transporting the brGDGTs into the Black Sea. We further quantify the so-called branched and isoprenoid tetraether (BIT) index (Hopmans et al., 2004) that compares the amount of brGDGTs to crenarchaeol (an isoprenoidal

* Corresponding author at: Senckenberg Biodiversity and Climate Research Centre BiK-F, Senckenberganlage 25, D-60325 Frankfurt am Main, Germany.
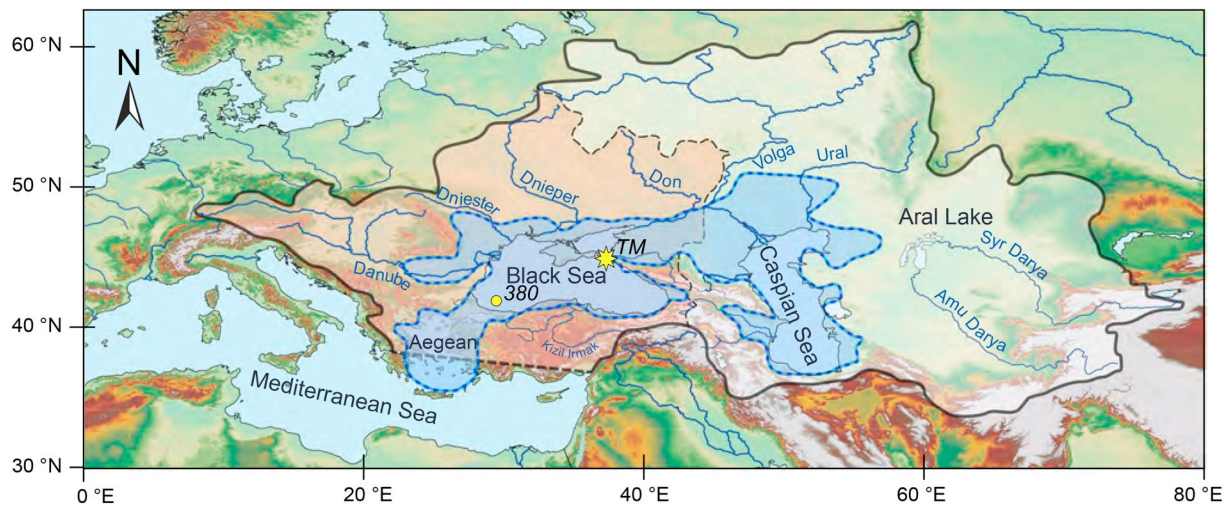 *E-mail address:* iuliana.vasiliev-popa@senckenberg.de (I. Vasiliev).

Fig. 1. Elevation map showing the extent of the late Miocene Black and Caspian Sea and their current drainage basins that largely overlaps with the drainage basin during the latest Miocene. The Paratethys extended over the Black Sea, Caspian Sea and potentially the Aegean Sea (e.g. Popov et al., 2016). Remark the uncertainty in the drainage basin around the Aegean Sea because of important rearrangement of the landmasses in the region since latest Miocene. Major rivers (Danube, Dniester, Dnieper, Don, Volga, Ural) draining into the Paratethys are indicated (modified after Grothe et al., 2016). Yellow star indicate Taman peninsula (TM) with Zheleznyi Rog section (Vasiliev et al., 2011, 2013). Yellow circle indicates DSDP core 42B Hole 380. (For interpretation of the references to colour in this figure legend, the reader is referred to the web version of this article.)

GDGT) in the Miocene-Pliocene record. The BIT index is a measure of the relative amount of aquatically produced versus soil-derived GDGTs and serves to monitor changes in the source of the organic matter (Hopmans et al., 2004). Additionally, we extend the δD record of organic biomarker of the Zheleznyi Rog section (Taman Peninsula; Vasiliev et al., 2011) into the latest Tortonian. This allows us to trace hydrological changes further back in time and to test whether the earlier evaporative phase recorded in the deep Black Sea basin (DSDP 42B 380; Vasiliev et al., 2015) can also be documented from the marginal facies exposed on Taman Peninsula. These long-term integrated records of input of organic matter, continental temperature, and soil pH indicate that there are two dry periods affecting the Black Sea region during the Tortonian- Messinian time interval. The data also indicate that the younger drying event (at 5.8 to 5.6 Ma) coincides with a period of significant continental cooling to the north of the Black Sea.

2. The Zheleznyi Rog section (Taman Peninsula, Russia)

The upper Miocene to lower Pliocene sedimentary successions of Zheleznyi Rog (northern Black Sea coast, Taman Peninsula, Russia; Fig. 1) represent a reference section for the Eastern Paratethys (Fig. 2) and have been subject to multiple studies covering biostratigraphy, magnetostratigraphy, cyclostratigraphy and radiometric dating that resulted in the establishment of an integrated stratigraphic time-frame (e.g. Chumakov, 1998; Chumakov et al., 1992; Pevzner et al., 2003; Popov et al., 2016; Semenenko, 1989; Krijgsman et al., 2010; Vasiliev

et al., 2011; Radionova et al., 2012; Grothe et al., 2014;). The sampled section comprises upper Tortonian, Messinian and lower Zanclean rocks (uppermost Khersonian, Maeotian, Pontian and Kimmerian in Eastern Paratethys terminology) roughly covering the time interval between ~8.7 and 4.8 Ma (Vasiliev et al., 2011). The basal part contains dark-grey clays alternating with yellowish sulfur films and diatomitic clays with ferruginous siltstones. Pyrite and secondary gypsum crystals, rare fish bones, juvenile ostracods shells, and foraminifera are observed. The middle part of the section is represented by alternations of grey-clays, whitish marls and diatomites and ends at −187 m with the last occurrence of the mollusk *Congeria novorossica* typical for the late Maeotian (early Messinian). A marine transgression and reconnection of the Black Sea to the Mediterranean Basin (Krijgsman et al., 2010) with deposition of grey marls and whitish diatomite layers characterizes the base of the Pontian (at ~6.1 Ma). This event was followed by re-establishment of brackish conditions in the Black Sea and a major invasion of species from Lake Pannon in Central Europe (Magyar et al., 1999; Stoica et al., 2013; Grothe et al., 2014). The upper part of the section shows alternations of grey-marls and whitish diatomite layers (Chang et al., 2014). A highly characteristic reddish layer at −92 m, with silty concretions, gypsum crystals and jarosite, followed by two meters of iron oxide-bearing oolithic sandstone marks a base-level drop that is hypothesized to be related to the sea level lowstand of the Mediterranean during the Messinian Salinity Crisis (5.60–5.33 Ma) (Roveri et al., 2014; Krijgsman et al., 2010). The upper 90 m of the section consist of Pliocene dark-grey marls with inter-bedded limonite

Fig. 2. Upper Miocene to lower Pliocene exposure at Zheleznyi Rog section located on Taman Peninsula, northern coast of the Black Sea basin (modified from Vasiliev et al., 2011).
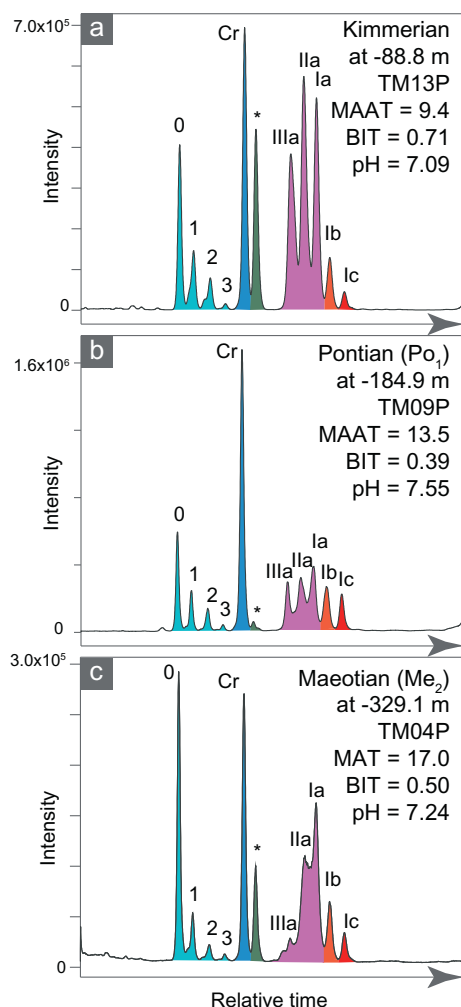
Fig. 3. HPLC-MS base peak chromatograms of GDGTs showing the distribution of isoprenoidal (0, 1, 2, 3) vs. branched (III, II, I, Ib, Ic) GDGTs. Cr = crenarchaeol while * denotes the C_{46} GDGT standard (198 ng in all samples). The examples are shown from young (a) to old (c), i.e. form upper Maeotian to Kimmerian. Stratigraphic levels are in meters. Note the relatively high contribution of branched GDGTs in panels (a) and (b). For each example the estimated mean annual air temperature (MAAT), branched and isoprenoid tetraether (BIT) index and paleo-soil pH are indicated.

layers and alternations of grey clays with coarser silts and sands.

3. Proxies for paleotemperature and paleohydrology

Several well established molecular biomarker proxies exist to reconstruct paleotemperatures in both marine and terrestrial settings (e.g. Brassell et al., 1986; Prahl and Wakeham, 1987; Schouten et al., 2013; Weijers et al., 2007a; Kim et al., 2008; Peterse et al., 2012). Transported terrestrial biomarkers (e.g. long chain *n*-alkanes, brGDGTs) may also be identified in marine settings (e.g. Peterse et al., 2009). To characterize the input of terrestrial organic matter in marine environments we use the BIT index (Hopmans et al., 2004) (Supplementary Fig. 1 and Fig. 3). Branched GDGTs are abundant in terrestrial settings, including soils and peats, whereas marine production of these compounds is very limited (e.g. Weijers et al., 2007a, Peterse et al., 2012) and hence the BIT index correlates with the relative amount of fluvial terrestrial input in marine sediments (Hopmans et al., 2004).

Over the past ten years significant advances have been made in the reconstruction of continental mean annual temperatures (MAAT) based on the relative distribution of brGDGT membrane lipids derived from bacteria thriving in soils (e.g.Weijer et al., 2007a; Peterse et al., 2012; De Jonge et al., 2014; Naafs et al., 2017) (Fig. 3 and Supplementary Fig. 1). The distribution of brGDGTs, expressed in the Methylation index of Branched Tetraethers (MBT) and the Cyclisation ratio of Branched Tetraethers (CBT), shows a significant linear correlation with modern MAAT in the range of −6 to 27 °C (Weijers et al., 2007a) (Supplementary Fig. 1).This approach has been used successfully to estimate continental MAAT in the geological past (e.g. Weijers et al., 2007b; Inglis et al., 2017; Mayser et al., 2017). As these membrane lipids are stable during transport by rivers into the oceans and are preserved during diagenesis, analysis of marine deposits close to the outflows of large rivers potentially provides continuous high resolution records of catchment-wide continental MAAT (Weijers et al., 2007b).

Some of the most frequently used biomarker molecules in paleoceanographic reconstructions are alkenones, long straight chain ketones synthesized by unicellular eukaryotic haptophyte prymnesiophyte algae, common in the photic zone of modern oceans (Marlowe et al., 1984; Volkman et al., 1980). Whereas the relative abundance of alkenones is used for temperature reconstructions, the hydrogen isotopic ratio of alkenones ($\delta D_{alkenones}$) has been shown to increase linearly with δD of water (δD_{water}; Englebrecht and Sachs, 2005; Paul, 2002). Here we use $\delta D_{alkenones}$ as a proxy for δD of Black Sea basin water.

Long-chain *n*-alkanes in the geologic record are typically derived from leaf waxes (Eglinton and Hamilton, 1967). These biomarkers record the δD of water used for the biosynthesis in the leaf. Several studies have shown that δD values of *n*-alkanes reflect the δD value of precipitation (e.g. Sachse et al., 2004a and b, Sachse et al., 2006), are affected by evapotranspiration operating in the plant (e.g. Sachse et al., 2004a and Sachse et al., 2004b; Sachse et al., 2012; Schimmelmann et al., 2016; Feakins and Sessions, 2010). Here, compound-specific δD data of long-chain *n*-alkanes ($\delta D_{n\text{-alkanes}}$) are interpreted to reflect the δD values of the original environmental water used by the higher plants and hence, serve as paleo precipitation/aridity proxies for the circum-Black Sea region.

4. Methods

We analyzed lipids from fifteen representative samples of the 475 m-long s Zheleznyi Rog section (Fig. 1). Samples were chosen from the marly and clayey intervals under the assumption of better preservation of organic matter in finer lithology. Sample spacing was arranged such that large scale changes in paleoenvironmental conditions and basin hydrology could be detected. All samples show excellently preserved biomarkers used in this study (Fig. 3 and 4).

4.1. Extraction, separation and analytical methods

All analytical steps were performed at the Organic Geochemistry laboratory of the Earth Sciences department, Utrecht University. Between 10 and 65 g of fresh sedimentary rock was dried and powdered. Organic compounds were extracted either using Accelerated Solvent Extraction (ASE) - (Dionex 200) equipment or Soxleth apparatus and dichloromethane (DCM)-methanol (9:1) solution. The total lipid extracts (TLE) were rotary-evaporated, transferred into 4 ml vials and subsequently rinsed over an anhydrous Na_2SO_4. Elemental sulfur was removed stirring the TLE dissolved in DCM with activated copper. The TLE were separated in different fractions using Al_2O_3 column chromatography using solvent mixtures of increasing polarity to elute the a-polar, less polar and polar fractions (details in Supplementary methods). Straight chain *n*-alkanes were isolated from the a-polar fraction using the urea-adduction, method that was repeated two to three times to eliminate the non-adductable alkanes from the a-polar fraction (details in Supplementary methods).
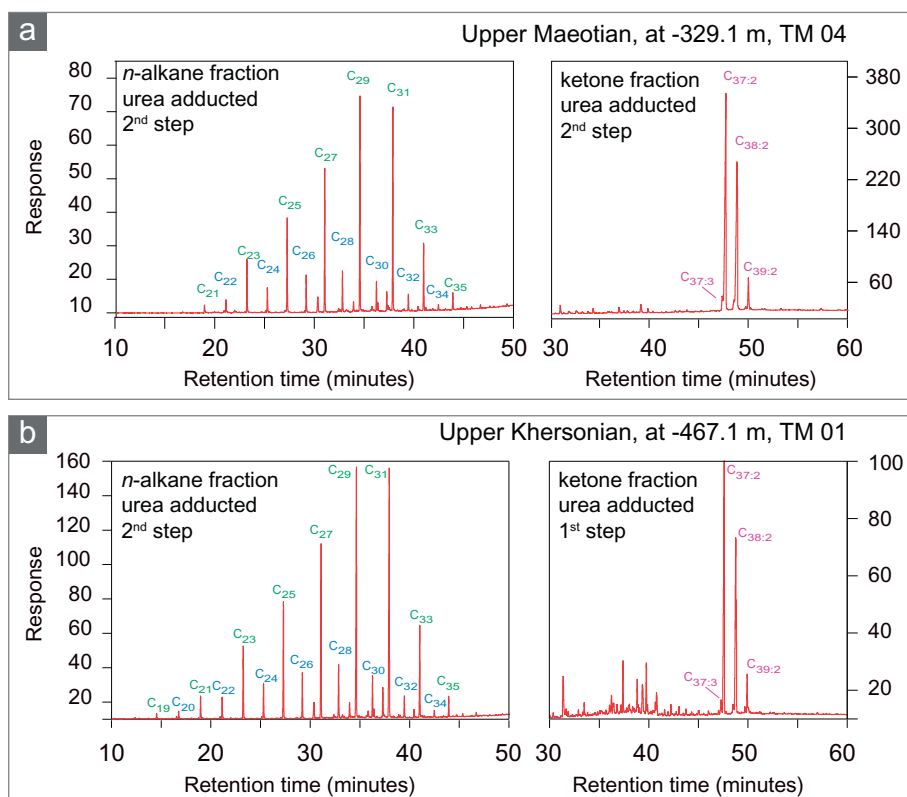
Fig. 4. GC-FID total-ion current chromatogram of purified *n*-alkane and alkenone fractions. C$_{17}$-C$_{34}$ refers to *n*-alkanes with odd (green) over even (blue) predominance in chain length distribution; C$_{37}$-C$_{39}$ (purple) are alkenones. a) TM 01 sample from upper Khersonian; b) TM 04 sample from upper Maeotian. (For interpretation of the references to colour in this figure legend, the reader is referred to the web version of this article.)

4.2. HPLC/MS analysis

The polar fraction was concentrated dissolved in *n*-hexane/2-iso-propanol (99:1, v:v) and filtered over a 0.4 μm PTFE filter prior to injection into a high performance liquid chromatography – atmospheric pressure chemical ionization/mass spectrometry (HPLC-MS) Hopmans et al. (2000). Analyses were performed using an Agilent 1290 Infinity series, 6130 Quadrupole UHPLC/MS equipped with auto-injector and Chemstation chromatography manager software. 10 μL of each polar fraction was injected and separation was achieved on an analytical Alltech Prevail Cyano column by elution with 90% *n*-hexane and 10% 9:1 (*v/v*) *n*-hexane:2-propanol (further details in Supplementary methods). Conditions for the Agilent 1290 series were are presented in the Supplementary Methods. Isoprenoidal and branched GDGT lipids were detected by scanning for their [M + H]$^+$ ion in selected ion monitoring (SIM) mode and quantified against a 198 ng of C$_{46}$ GDGT internal standard with an assumed equal ionization efficiency for the different compounds (Huguet et al., 2006). At some levels we verified results by repeating runs (see Table 1).

We achieved an excellent separation of the peaks (Fig. 3). The chemical structures of the used GDGTs and their [M + H]$^+$ are illustrated in Supplementary Fig. 1.

The relative input of soil organic matter in marine sediments was assessed using the branched and isoprenoid tetraether (BIT) index (Hopmans et al., 2004), calculated as:

$$BIT = \frac{[GDGT\ Ia + GDGT\ IIa + GDGT\ IIIa]}{[GDGT\ Ia + GDGT\ IIa + GDGT\ IIIa] + [Cren']}$$

The mean annual air temperature (MAAT) and pH, plotted in Fig. 5, were estimated according to Peterse et al. (2012) as follows:

$$MAAT = 0.81 - 5.67*CBT + 31.0*MBT'$$

$$pH = 7.90 - 1.97*CBT$$

MBT' and CBT are calculated as follows:

Table 1
BIT, MAAT and pH estimates. Calculation of MAAT and pH follows Peterse et al. (2012). Remark to good reproducibility of the indices for samples we analyzed multiple times as extra check (Vasiliev et al., 2018).

Sample code	Level (m)	BIT	CBT	MBT'	MAAT	pH
TM 02P	−405.0	0.58	0.34	0.59	17.23	7.23
TM 03P	−380.3	0.43	0.39	0.48	13.62	7.14
TM 04P	−329.1	0.50	0.34	0.58	16.99	7.24
TM 05P	−268.1	0.41	0.29	0.60	17.73	7.32
TM 06P	−240.0	0.42	0.25	0.42	12.35	7.40
TM 07P	−226.6	0.40	0.27	0.46	13.52	7.37
TM 09P	−184.9	0.39	0.18	0.44	13.53	7.55
TR 121P	−143.0	0.50	0.08	0.22	7.05	7.75
TM 10P	−133.6	0.50	0.11	0.27	8.52	7.68
TM 11P	−116.2	0.63	0.33	0.28	7.78	7.25
		0.57	0.25	0.32	9.32	7.40
		0.54	0.34	0.32	8.84	7.24
		0.55	0.23	0.33	9.80	7.45
TK 28P	−109.7	0.49	0.38	0.29	7.59	7.15
TK 21P	−104.6	0.60	0.27	0.26	7.25	7.37
		0.66	0.27	0.26	7.35	7.36
TM 12 P	−93.8	0.53	0.28	0.26	7.31	7.34
TM 13P	−88.8	0.71	0.41	0.35	9.37	7.09
TM 15P	−27.3	0.93	0.51	0.49	13.19	6.90

$$MBT' = \frac{[GDGT\ Ia + GDGT\ Ib + GDGT\ Ic]}{[(GDGT\ Ia + GDGT\ Ib + GDGT\ Ic) + (GDGT\ IIa + GDGT\ IIb + GDGT\ IIIb) + (GDGT\ IIIa)]}$$

$$CBT = -LOG \frac{[GDGT\ Ib + GDGT\ IIb]}{[GDGT\ IIa + GDGT\ IIa\ ]}$$

4.3. Gas chromatography and mass spectrometry analysis

The composition of individual *n*-alkanes and alkenones was analyzed by gas chromatography (GC), GC-mass spectrometry (GC/MS).
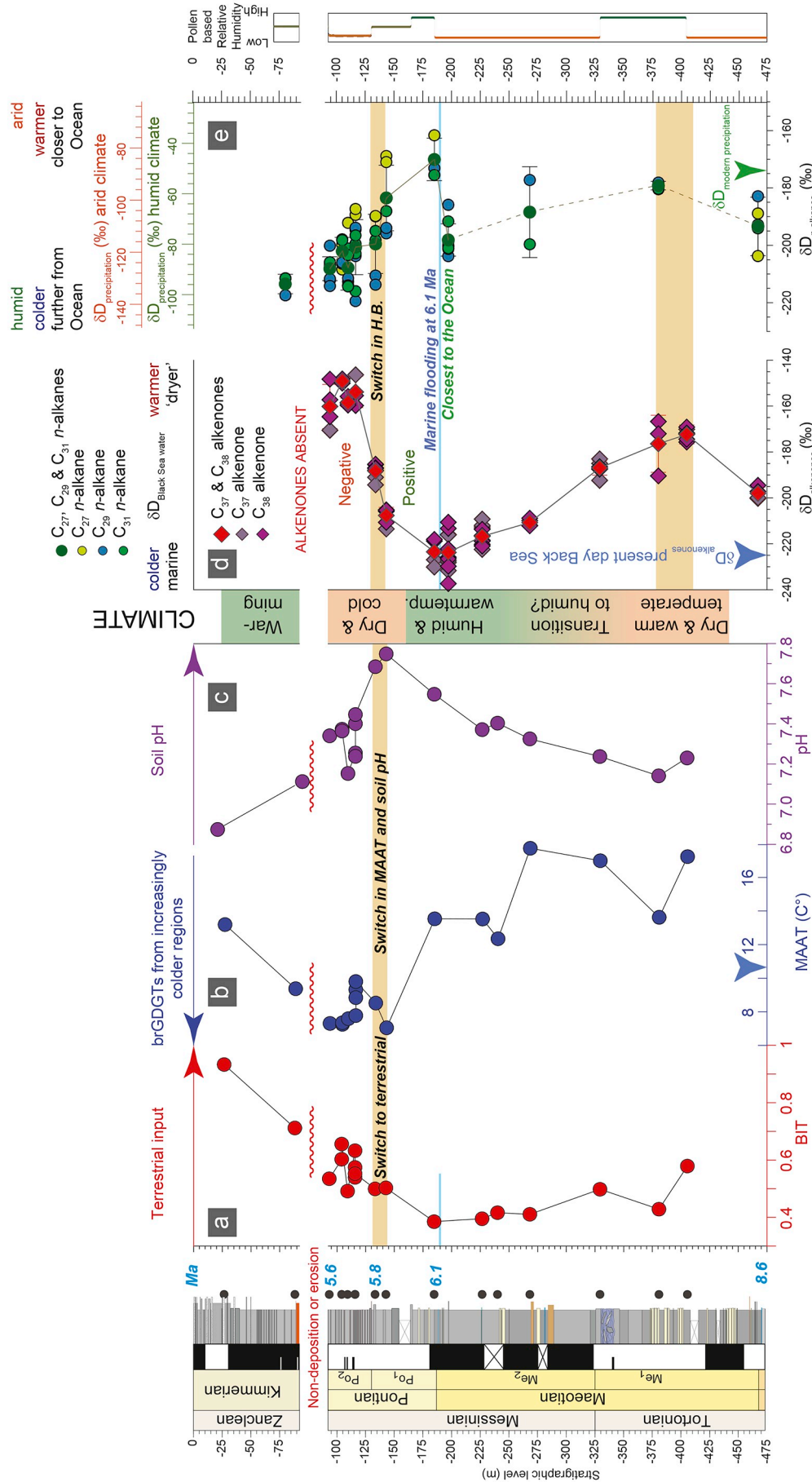
Fig. 5. Paleoenvironmental proxy data from Zheleznyi Rog. BIT index (a), brGDGT-based MAAT reconstruction (b), pH (c) and δD$_{n-alkane}$ (d) as well as δD$_{n-alkane}$ (e) data are presented within the framework of the Paratethys time scale including paleomagnetic data (Vasiliev et al., 2013). Maeotian, Pontian and Kimmerian regional stages are next to Tortonian, Messinian and Zanclean global stages. Ages in million years are from Krijgsman et al. (2010), Vasiliev et al. (2013) and Grothe et al. (2014). Relative humidity data are redrawn from Filippova (2002). δD precipitation values are colour-coded and calculated for two end-member scenarios 1) a European 'humid' temperate climate (green; using Sachse et al., 2006) and 2) a European 'arid' climate (orange; using Feakins and Sessions, 2010). HB stands for hydrological budget. The blue arrow in the MAAT bottom bar indicates the present-day MAAT value at the current location of the site. (For interpretation of the references to colour in this figure legend, the reader is referred to the web version of this article.)

Table 2

δD values of alkenones and *n*-alkanes. Average, number of measurements and standard error of the means (SEM) are listed; n.d denotes levels where δD was not determined. In italic letters are the data from Vasiliev et al. (2015) (Vasiliev et al., 2018).

Sample code	Level (m)	C_{37} & C_{38} alkenones			C_{37} alkenones			C_{38} alkenones			C_{29} & C_{31} *n*-alkanes			C_{27}, C_{29} & C_{31} *n*-alkanes		
		δD (‰)	N	SEM	δD (‰)	N	SEM	δD (‰)	N	SEM	δD (‰)	N	SEM	δD (‰)	N	SEM
TM 01	−467.1	−198.0	4	0.7	−200.1	2	7.0	−195.9	2	0.3	−190.8	4	2.7	−191.8	7	2.5
TM 02	−405.0	−172.2	7	1.2	−171.1	2	1.0	−172.7	5	0.9	n.d.			n.d.		
TM 03	−380.3	−176.4	3	0.1	n.d.			−176.4	3	0.1	−179.2	2	1.1	−177.9	4	1.8
TM 04	−329.1	−187.0	6	0.8	−186.8	3	0.4	−187.1	3	2.9	n.d.			n.d.		
TM 05	−268.1	−210.7	4	1.2	−211.0	2	1.0	−210.5	2	0.6	−188.4	2	11.2	−188.8	3	6.5
TM 07	*−226.6*	*−216.8*	*14*	*0.9*	*−215.6*	*7*	*0.5*	*−217.9*	*7*	*1.0*	*n.d.*			*n.d.*		
TM 08	*−197.1*	*−223.8*	*12*	*0.4*	*−223.9*	*5*	*0.3*	*−223.7*	*7*	*0.3*	*−197.2*	*6*	*2.8*	*−198.1*	*9*	*1.9*
TM 09	*−184.9*	*−223.5*	*4*	*0.3*	*−228.6*	*2*	*0.6*	*−218.5*	*2*	*2.9*	*−174.3*	*2*	*1.2*	*−170.1*	*3*	*4.3*
TR 121	*−143.0*	*−207.7*	*6*	*0.7*	*−208.0*	*3*	*0.4*	*−207.3*	*3*	*0.6*	*−190.3*	*4*	*2.8*	*−183.5*	*6*	*4.7*
TM 10	*−133.6*	*−188.3*	*7*	*0.8*	*−190.3*	*3*	*0.4*	*−186.8*	*4*	*1.8*	*−195.0*	*1*		*−195.0*	*1*	
TM 11	*−116.2*	*−153.9*	*3*	*0.3*	*−146.4*	*1*		*−157.6*	*2*	*0.5*	*−204.1*	*8*	*3.2*	*−200.6*	*12*	*2.8*
TK 28	*−109.7*	*−158.0*	*3*	*0.9*	*n.d.*			*−158.0*	*3*	*0.9*	*−209.7*	*3*	*4.3*	*−204.5*	*5*	*4.2*
TK 21	*−104.6*	*−149.1*	*2*	*1.1*	*n.d.*			*−149.1*	*2*	*1.1*	*−200.7*	*3*	*2.6*	*−202.1*	*5*	*2.2*
TM 12	*−93.8*	*−160.2*	*4*	*0.2*	*−170.6*	*1*		*−156.7*	*3*	*0.2*	*−207.8*	*6*	*2.0*	*−208.1*	*9*	*1.4*
TM 13	*−80.0*	*alkenones absent*			*alkenones absent*			*alkenones absent*			*−214.5*	*2*	*4.6*	*−213.5*	*3*	*2.0*

The *n*-alkanes and alkenones were identified using mass spectra, molecular ion mass and retention time using a Thermo-Finningan Trace Gas Chromatography (GC) Mass Spectrometer (Themo-Finningan Trace DSQ) (details in Supplementary methods)The a-polar components were identified by their spectra and quantified using the total ion current (Fig. 4a and b).

4.4. Compound-specific hydrogen isotope analysis

The compound-specific δD values of individual *n*-alkanes and alkenones were measured for five stratigraphic levels (TM 01 to TM 05) by injection of the purified fractions on a HP 6890 N Gas Chromatograph (GC) coupled to a Thermo-Finnigan Delta Plus XP Isotope Ratio Mass Spectrometer (GC-IRMS). GC-IRMS conditions, number of analysis and performance monitoring are presented in the supplementary methods. Each extract was measured between two and fourteen times. The average results for each *n*-alkane were plotted (Fig. 5). Error bars are based on the standard error of the means of the full set of multiple analyses.

5. Results

5.1. BIT index, MAAT and pH estimates based on soil derived branched GDGT lipids

The Zheleznyi Rog samples contain a wide range of branched and isoprenoidal GDGTs (Fig. 3 and Supplementary Fig. 1). The BIT index shows little variation between 0.4 and 0.6 over the interval between −400 to −175 m (Fig. 5 and Table 1). From −175 m upwards it shows a steady increase up to 0.93. Conventionally, for sediments with low terrestrial matter input and BIT index lower than 0.3, the TEX_{86} method can be applied for sea water temperature reconstructions (Hopmans et al., 2004). Conversely, sediments with BIT values ≥ 0.3 indicate a dominance of terrestrial organic matter which permits using brGDGTs for MAAT reconstructions. Well-defined brGDGT peaks were identified already from the base peak chromatogram indicative of a good separation per-component (Fig. 3 and Supplementary Fig. 1). The reconstructed MAAT values show large fluctuations, of almost 11 °C (Fig. 5). In the lower interval of the section values remain constant at around 16 °C. Above −270 m, the MAAT values decrease in two steps, from 16 to 12 °C at −250 m and towards 7 °C at −145 m (Fig. 5). Up to stratigraphic level −80 m, the values show little variation, remaining between 8 and 10 °C (Fig. 5).

Reconstructed soil pH values based on the CBT ratios of brGDGT lipids (after Peterse et al., 2012) steadily increase from 7.1 at −400 m

towards 7.8 at −145 m, values that are typical for slightly alkaline to moderately alkaline soils (Atlas of the Biosphere). Above −145 m, pH values suddenly drop to an average of 7.3 (Table 1 and Fig. 5).

5.2. Alkenones and n-alkanes

In the a-polar fractions of seventeen out of the fifteen levels studied we could identify long-chained (C_{37}-C_{39}) unsaturated ethyl and methyl ketones (alkenones), indicative for haptophyte algae (Fig. 4). The a-polar fractions of all samples contain *n*-alkanes ranging from *n*-C_{21} to *n*-C_{35}, with a strong predominance of odd-carbon number long-chain (C_{27}-C_{29}) *n*-alkanes (Fig. 5 and Vasiliev et al., 2013).

5.3. Compound specific hydrogen isotope analysis

5.3.1. Alkenone hydrogen isotope ratios

The hydrogen isotopic composition of the C_{37} and C_{38} alkenones ($\delta D_{alkenone}$) varies between −220‰ and −150‰, with two prominent high-value peaks in the $\delta D_{alkenone}$ record (Table 2 and Fig. 5). The older peak interval between -405 m and -375 m reaches values of −172‰, the younger peak interval (−130 to −90 m) attains highest values of −140‰. Lowest values are reached in the middle part of the succession with −230‰ at −200 m (Fig. 5). This implies a 70‰ increase in the $\delta D_{alkenone}$ values between −140 and −120 m (Fig. 5; Vasiliev et al., 2013). Samples TM 06 (at −240 m), TM 13 (at −88.8 m), TM 14 (at −66.5 m) and TM 15 (at −27.3 m) did not contain alkenones.

5.3.2. n-Alkane hydrogen isotope ratios

The δD values of C_{27}, C_{29} and C_{31} *n*-alkanes range from −214‰ to −170‰ ($\delta D_{n\text{-alkane}}$) (Table 2 and Fig. 5). The mean δD values of C_{27}, C_{29} and C_{31} *n*-alkanes stay rather constant in the lower part of the section. The highest values are recorded at −180 m. The values for the younger part of the section show a decreasing trend from ~ −170‰ to 214‰.

6. Discussion

6.1. BIT index, MAAT and pH estimates based on soil derived branched GDGT lipids

6.1.1. GDGT derived BIT index

Typical for coastal marine environments, BIT values in the Zheleznyi Rog section at all times lie between 0.40 and 0.93 (Hopmans et al., 2004; Table 1 and Fig. 5). BIT values vary around 0.45 up section from −405 m to −185 m, where the BIT value attains a minimum of
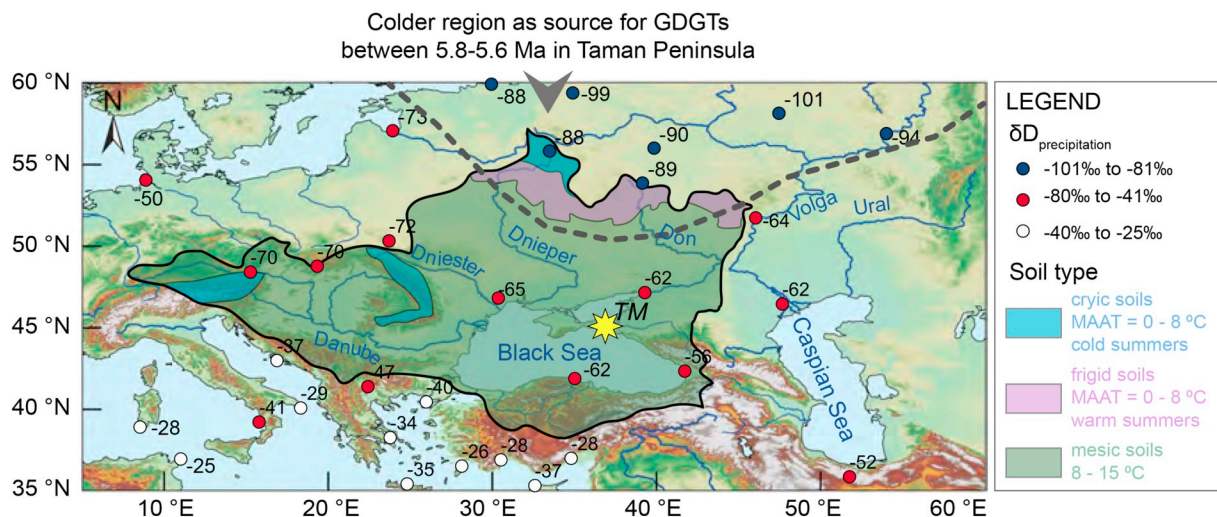
Fig. 6. Comparison of Zheleznyi Rog with deep sea records from the Black Sea Basin (DSDP 42B 380A) and northern hemisphere sea surface temperature records. Magnetostratigraphy follows Van Baak et al. (2016). δD_alkenone values are from Vasiliev et al. (2015). Northern hemisphere sea surface temperature anomalies (SST; 30°-50° N stack) are from Herbert et al. (2016); Pontian marine incursion is marked in both DSDP 380A and the Taman section by lower δD_alkenone values. MAAT values indicate cooling at 5.8 Ma almost time-equivalent with the negative SST anomaly recorded in the northern hemisphere stack.

Fig. 7. Present-day Black Sea drainage area and mean annual soil temperatures. The rivers draining into Black Sea (Danube, Dniester, Dnieper, Don) and Caspian Sea (Volga, Ural) are in blue. Map figure is modified after van Grothe (2016). Blue = cryic soil (MAAT = 0–8 °C; cold summers), purple = frigid soil (MAAT = 0–8 °C; warm summers) and green = mesic soil (MAAT = 8–15 °C). δD values of present-day precipitation are from IAEA (2001). Long-term means were calculated by selecting yearly means with data coverage > 75% for at least eight months. Blue circles indicate δD $_{precipitation}$ < −80‰, red circles indicate δD$_{precipitation}$ between −41‰ and − 80‰, white circles indicate δD $_{precipitation}$ > −40‰. The grey dotted line approximates the boundary between the colder and the temperate regions. (For interpretation of the references to colour in this figure legend, the reader is referred to the web version of this article.)

0.39 corresponding to a minimum in terrestrial organic matter input. This minimum is in agreement with a postulated inland change of the coast line previously inferred to a marine transgression at -185 m (Grothe et al., 2014). After this level, the BIT values gradually rise consistent with an increasing input of terrestrial organic matter into the Black Sea.

6.1.2. MAAT estimates based on soil derived branched GDGT lipids

The MBT′/CBT derived terrestrial MAAT records indicate variations of almost 11 °C (Fig. 5). The inferred decrease in MAATs from ~16 °C (−400 to −268 m) to ~8 °C (−143 to 93.8 m) occurs via two steps (from −268 m to −230 m and from −175 m to −143 m; Fig. 5).

The MAAT estimates of ~16 °C for the lower part of the section are higher compared to the average present-day values of 10–11 °C for the northern Black Sea coast at the current location of Zheleznyi Rog section, on Taman Peninsula. Conversely, MAAT estimates for the upper part of the section cluster around 8 °C, some 2–3 °C lower than present day values. Bearing in mind that there are large root mean square errors (RMSE) on absolute MBT′/CBT- derived MAAT reconstructions on the order of 5 °C (Peterse et al., 2012), we postulate a relative trend towards colder MAATs up section (Fig. 5). Local climate was previously estimated to be rather dry for most parts of the record based on the combined δD$_{alkenone}$ and δD$_{n-alkane}$ (Vasiliev et al., 2013). Using a recently developed aridity calibration would shift inferred temperatures to values that are ~2 °C higher (Yang et al., 2014) placing the late Miocene MAAT values of the upper part of the section in close proximity to the present day values. The MAAT signal of river-transported brGDGTs hence indicates similar climate conditions in the catchment area of the rivers feeding the Black Sea today.

The rapid, large magnitude, MAAT decrease from ~16 °C to ~8 °C between −175 m and − 143 m seems drastic given the relatively short amount of time (~0.4 Myr; Vasiliev et al., 2011). Two processes may be responsible for this rapid temperature change:

1) Sustained late Miocene cooling was found synchronously in both hemispheres, with ocean temperatures dipping to near-modern values between about 7 and 5.4 million years ago (Herbert et al., 2016; Fig. 6). The proposed mechanism for this late Miocene cooling is a reduction in atmospheric pCO_2 values, from above 500 to below 350 ppm. This period of maximum cooling coincides with evidence for transient glaciations in the northern hemisphere and with a steepening of the pole-

to-equator temperature gradient, as well (Deconto, 2003). Hence the here inferred change in MAAT for the continental Eurasian interior is in line with changes in the global oceans. Additionally, river water transporting the brGDGTs during the time interval between 6.1 and 5.7 could have been sourced as far north as regions of northern hemisphere glacial melt, which might add to the observed shift in temperatures.

2) As an alternative to global cooling, the source region for the river-transported brGDGT might have shifted over the time interval studied here. brGDGT are known to be transported over very long distances by rivers and, therefore, reflect an integrated signal of temperature changes in the drainage basin. With a size of 1.864.000 km^2 the present day Black Sea drainage basin covers important parts of central and eastern Europe and, to a lesser extent, northern Turkey (Ross et al., 1978; Fig. 7). Currently the drained area spans around 40° in longitude and 20° in latitude and the Danube River supplies 53% of the river input into the Black Sea. The Danube drains regions where MAAT varies around 9 to 10 °C. Today, only 4% of the fresh water discharge into the Black Sea comes from the south (Turkey) via the Sakarya River, draining regions with MAAT around 8 °C. Most of the other riverine input originates in the headwaters of Dnieper and Don, rivers that are draining much cooler regions (4 °C at 57°N to 10 °C at 45°N) than the Danube (Fig. 6). As the Black Sea was also connected to the Caspian Sea during the late Miocene (Van Baak et al., 2016, 2017) the brGDGT input into the Black Sea basin could also have been influenced by drainage basin changes of rivers feeding the Caspian Sea (Fig. 1). At present, the largest fresh water source (82%) for the Caspian Sea is the Volga that today drains even colder regions with MAAT < 4 °C. A contribution from a paleo-Volga River via the Caspian Sea can thus not be excluded and might have had a profound impact on reconstructed temperatures. Collectively, we, therefore, argue that the relative contribution of rivers transporting soil derived GDGTs into the Black Sea basin changed towards rivers, sourced in colder regions to the north of the Black Sea basin.

6.1.3. pH estimates based on soil derived brGDGT lipids

The calculated soil pH values mimic the trend recorded in the MAAT estimate, with pH values increasing until the maximum value of 7.7 (−150 m) at the same level where calculated MAAT is lowest. After that level the pH values decrease until reaching a minimum value of 6.9 (at −27.3 m). Bearing in mind the RMSE = 0.8 on CBT- derived pH

reconstructions (Peterse et al., 2012) we would like to put strain on the relative changes in the calculated pH (Fig. 5).

The calculated soil pH values are, except the upper most value, typical for rather neutral to slightly alkaline soils and, therefore, consistent with a catchment area covered largely by alkaline soils. Such conditions, with soils classified as mildly alkaline (pH of 7 to 8), are today present in the catchments of Dnjepr and Don Rivers (Atlas of the Biosphere). Both are draining regions of almost exclusively alkaline soils, covered by steppe-type vegetation, adapted to drier conditions with precipitation less than between 100 and 500 mm/year (e.g. Breckle, 2002). A contribution from the paleo-Volga River via the Caspian Sea connection to the Black Sea could provide an additional source for alkaline pH values. The present day Volga drains regions covered almost exclusively by alkaline soils/steppe vegetation with precipitation values < 350 mm/year. The calculated pH values of 7.1 to 7.7 for the main part of the section fit best to regions equivalent in soil pH (i.e. reflected also in type of steppe vegetation) typically found now on the northern coast of the Black Sea, in the drainage basins of Dniestr, Dnjepr and Don rivers. Additionally, the low MAATs point also towards colder northern latitude as origin for the brGDGTs. The highest pH values of 7.7 (i.e. more arid conditions) coincide with the previously recorded switch towards a negative hydrological budget for the region based on the δD values of *n*-alkanes (Vasiliev et al., 2013).

6.2. Alkenones and n-alkane biomarkers

Several intervals of the Zheleznyi Rog section contain varying relative contribution of long-chain (C_{37}-C_{39}) alkenones (Fig. 4) indicative for haptophyte algae. The relative distribution of C_{37}, C_{38} and C_{39} alkenones suggests a marine origin (Fig. 4; e.g. Prahl and Wakeham, 1987). $C_{37:4}$ could not be identified in any of the samples. The a-polar fractions of all samples contain a series of *n*-alkanes ranging from *n*-C_{21} to *n*-C_{35}, with the long-chain (C_{27}-C_{29}), predominantly odd-carbon number homologues, prevailing (Fig. 4). This is a typical signature for terrestrial higher plant derived *n*-alkanes (Eglinton and Hamilton, 1967), indicating an important terrestrial organic matter input.

6.2.1. Compound specific hydrogen isotope (δD) analysis: alkenones

The hydrogen isotopic compositions of C_{37} and C_{38} alkenones ($\delta D_{alkenone}$) cover a large range between −220‰ (typical for marine settings) and − 147‰. Most prominent are two peaks with elevated $\delta D_{alkenone}$ values (−405 m and – 140 to −120 m; Table 2 and Fig. 5). The earlier peak in $\delta D_{alkenone}$ (at −405 m in the section) attains −172‰, about 25 to 35‰ higher than the section intervals below and above. The BIT value corresponding to the older peak in $\delta D_{alkenone}$ (although for only one sample), is consistent with more coastal marine values. The MAAT value is in the high temperature range while the pH value indicates that the brGDGTs were originating from alkaline soils.

The younger positive peak in $\delta D_{alkenone}$ is reflected by a ca. 70‰ increase between −140 to −120 m of section (Fig. 5). This positive $\delta D_{alkenone}$ excursion was previously interpreted as a shift towards very dry, D enriching, conditions in the Black Sea and the Mediterranean during the MSC (Vasiliev et al., 2013, 2017). The high $\delta D_{alkenone}$ values start when BIT values change towards more coastal values, MAAT values decrease and reconstructed pH is reaching its maximum value (Fig. 5). At this interval, all proxies are in line indicating a relatively rapid onset of a cold and dry phase. The inferred switch in the hydrological balance towards dry conditions may hence have been forced by the colder climate that was established at the time in the northern Black Sea region.

The lowest $\delta D_{alkenones}$ values (of −220‰) are recorded at −180 m, coinciding with the lowest BIT values and relatively high MAATs. All arguments suggest that these $\delta D_{alkenone}$ values which are typical for marine environments correspond with the timing of the marine flooding in the region (Krijgsman et al., 2010; Grothe et al., 2014).

6.2.2. Compound specific hydrogen isotope (δD) analysis: n-alkanes

δD values of the long chain *n*-alkanes (C_{27}, C_{29} and C_{31}) show large variations over time. For example, for the C_{29} *n*-alkanes the δD varies by 46‰, from as low as −219‰ (between −150 m and − 90 m) to −173‰ (at −180 m) (Table 2 and Fig. 5). These high $\delta D_{n\text{-alkane}}$ values coincide with the lowest $\delta D_{alkenone}$ values, and with the lowest BIT values, event preceding the cooling step inferred from MAAT estimates (Fig. 5). This suggests that a marine flooding event changed the proximity of the coastal line, generating important changes in the entire hydrological system in the region by the close vicinity of the water vapor source, consequently affecting the $\delta D_{precipitation}$ values and implicitly the $\delta D_{n\text{-alkanes}}$.

Our $\delta D_{n\text{-alkanes}}$ record shows a clear trend towards increasingly lower values, which might indicate that precipitation, was: 1) falling further inland, 2) falling in a colder region or 3) indicating a more humid period. The data presented here allow for the first time explaining the mechanisms behind the low $\delta D_{n\text{-alkanes}}$ values in the Taman record. The lower $\delta D_{n\text{-alkanes}}$ values, combined with the increasingly higher input of terrestrial organic matter (vs. in-situ produced/preserved), inferred from the BIT values, suggest that there has been a shift with precipitation falling increasingly further inland (Fig. 5). This, in combination with an increasing latitudinal temperature gradient enhancing fractionation, results in more fractionated $\delta D_{n\text{-alkanes}}$ values of the n-alkanes transported from further north to the Black Sea basin (Fig. 5 and 7). The lower $\delta D_{n\text{-alkanes}}$ are recorded during times of high $\delta D_{alkenones}$ (Fig. 5) that would indicate overall dryer conditions with more evaporation than precipitation and hence less river input. Also the soil pH values are in line with a drier and/or more northern source for the soil organic matter as the CBT values are typical for more alkaline soils. Based on the combined proxies, we infer that the Taman region was becoming drier, colder and receiving fresh water from more northern latitudes (Fig. 7) strongly suggesting a gradual shift towards a more continental climate conditions.

The argumentation above assumes that the $\delta D_{precipitation}$ values are directly related to $\delta D_{n\text{-alkane}}$, with a constant biosynthetic fractionation of 157‰ between source water and *n*-alkane (Sachse et al., 2006; Sessions et al., 2004), whereas an additional evapo-transpiration effect (up to ~60‰) has been found for arid ecosystem (Feakins and Sessions, 2010). Taking this effect in account, the calculated $\delta D_{precipitation}$ for the dry and cool interval would have varied between −132 and − 80‰, values exclusively observed in cold northern high latitudes in Eurasia (IAEA, 2001) and hence in line with our interpretation (Fig. 5 and 7). Accordingly, we suggest that the catchment of the riverine water must have reached further northern (i.e. colder) region than today.

7. The new proxy data in a chronologic framework

In the past seven years, age constraints for the Zheleznyi Rog section have led to a better understanding of the timing of the events that affected the Black Sea basin. One of the robust tie points relates to the ash located at the base of the section (just below the level − 470 m) that is dated at 8.6 Ma (Fig. 2 and 5) (Vasiliev et al., 2011). The Khersonian-Maeotian transition is refined by Popov el al., (2016) and placed at the level of a (initially considered minor) fault located one meter above the dated ash (Fig. 5). The Khersonian/Maeotian boundary thus most likely corresponds to a hiatus in the succession of Zheleznyi Rog.

Another well-documented event is the 6.1 Ma Pontian transgression, located at −196 m (Krijgsman et al., 2010; Vasiliev et al., 2011; Chang et al., 2014). Between these two tie points, the time frame is complicated by several hiatuses (see Vasiliev et al., 2011). In the present time frame the boundary between the lower and upper Maeotian is placed at the top of the breccia layer at −330 m and correlated to the base of C3An and an age of ~6.7 Ma (Rostovtseva and Rybkina, 2017).

7.1. Upper Tortonian-lower Messinian (8–6.7 Ma; lower Maeotian): Dry and warm climate in the entire Black Sea region

The lower part of the section, corresponding to the upper Tortonian-lowermost Messinian, is marked by relatively higher $\delta D_{alkenones}$ values (around −170‰), consistent with a relatively dry phase and with warm MAAT of 15 °C. Our biomarker based record is corroborated by palynology showing that the lower Maeotian was a semiarid phase, with widespread herbaceous-dwarf shrub xerophilous Chenopodiaceae groups (Popov et al., 2016). Vegetation reconstructions indicate dry and warm climate with environments typical for a saline-steppe and semi-arid deserts (Filippova, 2002; Ivanov et al., 2010; Syabryaj et al., 2007).

Dry climate conditions for the Khersonian and the beginning of the Maeotian are also reported from the Dacian basin (Paratethys, west of the Black Sea), marked by paleosoils (Vasiliev et al., 2004) containing carbonate nodules, requiring strong seasonality and relatively dry climate. Additional precipitation reconstructions based on amphibians and reptilians show low rainfall values in the entire Paratethys region (Böhme et al., 2011). The late Miocene mammal records of southeast Europe reveal changes to faunas better adapted to a dry climate and open terrain (Korotkevich, 1989; Lungu, 2008; Koufos, 2006; Eronen et al., 2009). This dry period is marked by higher $\delta D_{alkenones}$ values and was most probably the direct result of a major sea-level lowstand in the Paratethys area during the Khersonian-Maeotian (Popov et al., 2010).

The $\delta D_{alkenones}$ data of the deep sea record of DSPD 42B Hole 380 hole also indicate dry conditions during the Khersonian-Maeotian (Vasiliev et al., 2015). Comparing the two independent biomarker records, one from a deep and one from a marginal setting of the Black Sea, it becomes clear that the exceptional dry phase is representative for the entire Black Sea region (Fig. 6).

7.2. Lower and middle Messinian (6.7–6.1 Ma; upper Maeotian): Wet and warm climate in the northern Black Sea

Our data indicate a wet and warm regional climate in the northern Black Sea during the lower Messinian/upper Maeotian. Estimated brGDGTs based temperatures fluctuate around 15 °C, 4 °C warmer than present day (Fig. 5). Combining MAAT estimates with the more negative $\delta D_{n\text{-}alkanes}$ data indicates that climate was more humid at the same time. This is in line with other paleoclimate data that suggests that lower Messinian MAAT in Europe was at least 5–8 °C warmer than pre-industrial age values, receiving around 400 mm/year more precipitation (Pound et al., 2011). Humid to sub-humid climates through major parts of Europe are also suggested by mammal hypsodonty data (Eronen et al., 2011; Fortelius et al., 2002), small-mammal community (van Dam et al., 2006) structure and herpetofaunal composition (Böhme et al., 2008). Fossil plant based climate reconstructions show that Europe had mostly humid to sub-humid summers (Quang et al., 2014).

Mayser et al. (2017) use similar approaches based on MBT′/CBT-derived MAAT reconstructions on lower Messinian (6.5–6.0 Ma) marine successions from Cyprus (Eastern Mediterranean). Their reconstructed MAAT-values are around 18 °C, which is 3 °C higher than our estimated MBT′/CBT-derived MAAT for the same time interval in Taman. This difference in the MAAT corresponds well to the 10° latitudinal difference, with Cyprus being located at 35°N while Taman is at 45°N.

7.3. Upper Messinian (6.1–5.6 Ma, Pontian): dry and cold climate in the northern Black Sea

The exceptionally high $\delta D_{alkenones}$ values (−147‰) coinciding with episodes characterized by increased terrestrial organic matter influx (i.e higher BIT) and colder conditions points to a dry and cold climate during the late Messinian. This time span is marked by northern hemisphere glacial cycles (e.g. TG 12–14 to TG 20–22) (Fig. 5). The substantial cooling apparently resulted in the significant, > 45‰, drop in the $\delta D_{n\text{-}alkanes}$ (to −210‰) (Fig. 5). This interval, where colder and drier conditions are inferred, is immediately followed by the highly characteristic reddish layer appearing at −92 m supporting the hypothesis that it could represent the expression of the sea level lowering during the MSC (5.60–5.33 Ma) (Krijgsman et al., 2010).

There are three possible mechanisms for the colder MAAT estimates, related to the fact that these lipids derive from soil bacteria and are hence brought to the marine realm by the river water. These alternative mechanisms are: 1) MBT′/CBT indices yield relatively low MAATs in arid settings (Peterse et al., 2012; Yang et al., 2014); 2) the riverine source for the brGDGT is physically changing from rivers draining warmer regions to rivers draining cold regions and 3) the overall regional climatic conditions are changing to much colder temperatures.

In the present day situation there a large difference between the recorded sea surface temperatures (SST) and MAAT (e.g. NOAA, 2017; Atlas of the Biosphere) in the Azov Sea, just north of Taman. The SST contour lines are recording values of 6 to 8 °C at the mouth of the Don River and reach 10 to 12 °C at the Kerch Strait, where the Azov Sea connects to the Black Sea (NOAA, 2017). These SST values are, at some places, at least 4 °C lower that the MAAT values. The same decoupling of the SST from MAAT is observed in the Caspian Sea where the SST in the northern part reaches only 4 to 6 °C, while the MAAT is 8 to 12 °C. The best explanation for this discrepancy is that the influx of riverine water (Don, Dnepr and Volga) originating in colder northern regions lowers the SST in these intracontinental basins.

The second explanation implies that the source for the riverine brGDGTs has changed from a southern and/or western source (e.g. draining warmer Turkey and/or Central Europe) to a northern source (Don and Dnepr or Volga). Such a change would require that the dominant source for riverine water to be the warmer southern regions or at least the warm enough regions drained by the paleo-Danube at that time. This assumption seems to be less likely since the surface of Anatolia (the possible southern source for riverine water) was significantly smaller than area drained by the northern rivers (Fig. 7). The Paleo-Danube contribution would bring soil lipids from region that were covered by temperate deciduous forests during the late Miocene, with temperatures modelled to be 2 °C warmer than today (Micheels et al., 2007). The temperate deciduous forests of today are developed on soils that are at least mildly to even strong acidic. We see a gradual change in the reconstructed pH and, next to the MAAT change we can infer a stronger western contribution in the soil lipids brought to Taman, although from a considerable distance.

The third alternative takes into consideration that this dry and cold period recorded from the northern Black Sea region coincides conspicuously with a general late Miocene cooling of the northern hemisphere (Herbert et al., 2016). In their SST anomaly record stacked from the Northern Atlantic ODP sites they document a maximum peak in late Miocene cooling trend of the northern hemisphere (Fig. 6). This specific cooling starts at 6.15 Ma and peaks at the lowest temperature in the interval 5.8 and 5.7 Ma. When comparing our MAAT cooling record to the Northern Atlantic SST anomaly (Herbert et al., 2016) we observe a striking similarity in the time of occurrence. It seems that the two cooling peaks from Northern Atlantic SST stack and the Taman (Black Sea) start simultaneously, at 5.8 Ma (Fig. 6). Therefore, a change of terrestrial organic matter (i.e. brGDGT) input originating from a colder drainage basin could be effectively caused by the northern hemisphere peak in cooling at 5.8 Ma. Alternatively, it may also reflect regional sea level change, restricting the Azov/Taman basin from the Black Sea. In this case the brGDGTs were brought almost exclusively form Don and Dnjepr, rivers draining the northern, colder Black Sea region.

7.4. Warm climate in the northern Black Sea at the beginning of Pliocene

Alkenones are absent in the Pliocene (Kimmerian stage within Zanclean) part of the section while the $\delta D_{n\text{-}alkane}$ data are limited to one

data point, with values typical for humid/colder/further-form-the-ocean values (Fig. 5 and 6). The MAAT data suggest warming taking place while BIT reaches values typical for mainly terrestrial derived organic matter, transported by rivers draining more acidic soils. Although the data are limited, this suggests that the early Pliocene in the circum Black Sea area was characterized by a return to warmer conditions.

8. Conclusions

Integrated analysis of organic geochemistry data from the upper Miocene and lower Pliocene deposits from Zheleznyi Rog (Taman Peninsula, Russia) shows large environmental changes surrounding the Black Sea basin continental realm:

1) There is a dry period during the Tortonian-earliest Messinian (Khersonian-Maeotian) expressed through very high $\delta D_{alkenones}$ values. This dry period is tentatively correlated to the conditions recorded in DSDP 42B 380 (interval 934–830 mbsf; Vasiliev et al., 2015) suggesting that the entire Black Sea basin experienced dry conditions.

2) Our data indicate a much wetter and warmer regional climate north of the Black Sea during the lower Messinian (upper Maeotian) than today. Estimated temperatures using brGDGTs indicate MAAT around 15 °C and the $\delta D_{n\text{-}alkane}$ data indicate that the region must have been more humid. These estimates agree with other climatic data indicating that the early Messinian in Europe was at least 5–8 °C warmer compared to pre-industrial times.

3) Our MAAT, BIT and pH data indicate that the drying event at 5.8 to 5.6 Ma inferred from $\delta D_{alkenone}$ data (Vasiliev et al., 2013) coincides with a period of significant continental cooling to the north of the Black Sea. During that time the Taman region was relatively dry and cold and was receiving fresh water from colder, steppe environments developed on alkaline soils north of the Black Sea region. This cooling period was probably responsible for the large (> 45‰) drop in $\delta D_{n\text{-}alkanes}$ values during the Pontian stage.

4) The 5.8–5.6 Ma dry and cold period coincides with Late Miocene cooling of the northern hemisphere documented (e.g. Herbert et al., 2016). Therefore, an alternative explanation to a changing source region for GDGTs could be northern hemisphere Late Miocene cooling that culminated with the buildup of the ephemeral, northern hemisphere, glaciation between 6.0 and 5.5 Ma (Holbourn et al., 2018).

5) The Pliocene time interval covered in the Zheleznyi Rog section is marked by warmer conditions and lower soil pH indicating a revival of the climatic conditions that characterized the Black Sea during the late Messinian.

Acknowledgements

Appendix A. Supplementary data

Supplementary data to this article can be found online at https://doi.org/10.1016/j.gloplacha.2018.10.016.

References

Böhme, M., Ilg, A., Winklhofer, M., 2008. Late Miocene "washhouse" climate in Europe. Earth Planet. Sci. Lett. 275, 393–401.

Böhme, M., Winklhofer, M., Ilg, A., 2011. Miocene precipitation in Europe: temporal trends and spatial gradients. Palaeogeogr. Palaeoclimatol. Palaeoecol. 304, 212–218.

Brassell, S.C., Eglinton, G., Marlowe, I.T., Sarnthein, M., Pflaumann, U., 1986. Molecular stratigraphy: a new tool for climatic assessment. Nature 320, 129–133.

Breckle, S.-W., 2002. Walter's Vegetation of the Earth. In: The Ecological Systems of the Geo-Biosphere, 4th ed. Springer, Berlin.

Chang, L., Vasiliev, I., Van Baak, C.G.C., Krijgsman, W., Dekkers, M.J., Roberts, A.P., Fitz Gerald, J.D., Van Hoesel, A., Winklhofer, M., 2014. Identification and environmental interpretation of diagenetic and biogenic greigite in sediments: a lesson from the Messinian Black Sea. Geochem. Geophys. Geosyst. 15, 3612–3627. https://doi.org/10.1002/2014GC005411.

Chumakov, I.S., 1998. The Problem of the Miocene-Pliocene Boundary in the Euxinian Region. Stratigraphy and Geological Correlation. vol. 8. pp. 396–404.

Chumakov, L.S., Byzova, S.L., Ganzey, S.S., Arias, C., Bigazzi, G., Bonadonna, F.P., Hadler-Neto, J.C., Norelli, P., 1992. Interlaboratory Fission Track Dating of Volcanic Ash Levels from Eastern Paratethys: A Mediterranean-Paratethys Correlation. Palaeogeography, Palaeoclimatology, Palaeoecology. (287–285).

De Jonge, C., Hopmans, E.C., Zell, C.I., Kim, J.-H., Schouten, S., Sinninghe Damsté, J.S., 2014. Occurrence and abundance of 6-methyl branched glycerol dialkyl glycerol tetraethers in soils: Implications for palaeoclimate reconstruction. Geochim. Cosmochim. Acta 141 (97–112), 2014.

Deconto, R.M., Pollard, D., 2003. Rapid Cenozoic glaciation, of Antarctica induced by declining atmospheric CO_2. Nature 421, 245–248.

Eglinton, G., Hamilton, R.J., 1967. Leaf Epicuticular Waxes. Science 156, 1322–1335.

Englebrecht, A.C., Sachs, J.P., 2005. Determination of sediment provenance at drift sites using hydrogene isotopes and unsaturation ratios in alkenones. Geochim. Cosmochim. Acta 69 (17), 4253–4265.

Eronen, J.T., Ataabadi, M.M., Micheels, A., Karme, A., Bernor, R.L., Fortelius, M., 2009. Distribution history and climatic controls of the late Miocene Pikermian chronofauna. Proc. Natl. Acad. Sci. 106, 11867–11871.

Eronen, J., Micheels, A., Utescher, T., 2011. A comparison of estimates of mean annual precipitation from different proxies: a pilot study for the European Neogene. Evol. Ecol. Res. 13, 851–867.

Feakins, S.J., Sessions, A.L., 2010. Controls on the D/H ratios of plant leaf waxes in an arid ecosystem. Geochim. Cosmochim. Acta 74, 2128–2141.

Filippova, N.Y., 2002. Spores, Pollen, and Organic-Walled Phytoplankton from Neogene Deposits of the Zheleznyi Rog Reference Section (Taman' Peninsula). Stratigr. Geol. Correl. 10, 176–188.

Fortelius, M., Eronen, J.T., Jernvall, J., Liu, L., Pushkina, D., et al., 2002. Fossil mammals resolve regional patterns of Eurasian climate change over 20 million years. Evol. Ecol. Res. 4, 1005–1016.

Grothe, A., 2016. The Messinian Salinity Crisis: a Parathethyan Perspective. Utrecht University, Utrecht, pp. 151 PhD Thesis.

Grothe, A., Sangiorgi, F., Mulders, Y.R., Vasiliev, I., Reichart, G.-J., Brinkhuis, H., Stoica, M., Krijgsman, W., 2014. Black Sea desiccation during the Messinian Salinity Crisis: Fact or fiction? Geology 42, 563–566. https://doi.org/10.1130/G35503.1.

Herbert, T.D., Lawrence, K.T., Tzanova, A., Cleaveland-Peterson, L., Gabalero-Gill, R., Kelly, K.S., 2016. Late Miocene global cooling and the rise of modern ecosystems. Nat. Geosci. 9, 843–847.

Holbourn, A.E., Kuhnt, W., Clemens, S.C., Kochhann, K.G.D., Jöhnck, J., Lübbers, J., Andersen, N., 2018. Late Miocene climate cooling and intensification of southeast Asian winter monsoon. Nat. Commun. 9, 1584.

Hopmans, E.C., Schouten, S., Pancost, R.D., van der Meer, M.J.T., Sinninghe Damsté, J.S., 2000. Analysis of intact tetraether lipids in archaeal cell material and sediments using high performance liquid chromatography/atmospheric pressure ionization mass spectrometry. Rapid Commun. Mass Spectrom. 14, 585–589.

Hopmans, E.C., Weijers, J.W.H., Schefuß, E., Herfort, L., Sinninghe Damste, J.S., Schouten, S., 2004. A novel proxy for terrestrial organic matter in sediments based on branched and isoprenoidtetraether lipids. Earth Planet. Sci. Lett. 224, 107–116.

Huguet, C., Hopmans, E.C., Febo-Ayala, W., Thompson, D.H., Sinninghe Damsté, J.S., Schouten, S., 2006. An improved method to determine the absolute abundance of glycerol dibiphytanyl glycerol tetraether lipids. Org. Geochem. 37, 1036–1041.

IAEA, 2001. GNIP Maps and Animations. International Atomic Energy Agency, Vienna. http://isohis.iaea.org.

Inglis, G.N., Collinson, M.E., Riegel, W., Wilde, V., Farnsworth, A., Lunt, D.J., Valdes, P., Robson, B.E., Scott, A.C., Lenz, O.K., Naafs, B.A., Pancost, R.D., 2017. Mid-latitude continental temperatures through the early Eocene in western Europe. Earth Planet. Sci. Lett. 460, 86–96.

Ivanov, D., et al., 2010. Miocene vegetation and climate dynamics in Eastern and Central Paratethys (Southeastern Europe). Palaeogeogr. Palaeoclimatol. Palaeoecol. 304, 262–275.

Kim, J.H., Schouten, S., Hopmans, E.C., Donner, B., Sinninghe Damste, J.S., 2008. Global sediment core-top calibration of the TEX86 paleothermometer in the ocean. Geochim. Cosmochim. Acta 72, 1154–1173.

Korotkevich, E.L., 1989. Zavershayuschie etapy razvitiya gipparionovoi fauny Vostochnoi

vropy. In: Yanshyn, A.L. (Ed.), Chetvertichyi Period, Paleontologiya i arkheologiya. Stiintsa, Kishinev, pp. 32–37 (in Russian).

Koufos, G.D., 2006. Palaeoecology and chronology of the Vallesian (late Miocene) in the Eastern Mediterranean region. Palaeogeogr. Palaeoclimatol. Palaeoecol. 234, 127–145.

Krijgsman, W., Stoica, M., Vasiliev, I., Popov, V.V., 2010. Rise and fall of the Paratethys Sea during the Messinian Salinity Crisis. Earth Planet. Sci. Lett. 290, 183–191.

Lungu, A., 2008. Le developpement de la faune de Hipparion dans le Sarmatien sur le territoire de la République de Moldova. Acta Palaeontologica Romaniae 6, 181–186.

Magyar, I., Geary, D.H., Müller, P., 1999. Paleogeographic evolution of the late Miocene Lake Pannon in Central Europe. Palaeogeogr. Palaeoclimatol. Palaeoecol. 147, 151–167.

Marlowe, I.T., et al., 1984. Long-chain (n-C$_{37-39}$) alkenones in the Prymnesiophyceae. Distribution of alkenones and other lipids and their taxonomic significance. Br. Phycol. J. 19, 203–216.

Mayser, J.P., Flecker, R., Marzzochi, A., Kouvernhoven, T.J., Lunt, D.J., Pancost, R.D., 2017. Precession driven changes in terrestrial organic matter input to the Eastern Mediterranean leading up to the Messinian Salinity Crisis. Earth Planet. Sci. Lett. 462, 199–211.

Micheels, A., Bruch, A.A., Uhl, D., Utescher, T., Mosbrugger, V., 2007. A late Miocene climate model simulation with ECHAM4/ML and its quantitative validation with terrestrial proxy data. Palaeogeogr. Palaeoclimatol. Palaeoecol. 253, 251–270.

Naafs, B.D.A., Inglis, G.N., Zheng, Y., Amesbury, M.J., Biester, H., Bindler, R., et al., 2017. Introducing global peat-specific temperature and pH calibrations based on brGDGT bacterial lipids, 2017, Introducing global peat-specific temperature and pH calibrations based on brGDGT bacterial lipids. Geochimica Cosmochimica Acta 208, 285–301.

NOAA, 2017. Operational SST Anomaly Charts for 2017. http://www.ospo.noaa.gov/Products/ocean/sst/anomaly/.

Palcu, D., Golovina, L., Vernyhorova, Yu., Popov, S.V., Krijgsman, W., 2017. Middle Miocene paleoenvironmental crises in Central Eurasia caused by changes in marine gateway configuration. Glob. Planet. Chang. 158, 57–71.

Paul, H.A., 2002. Application of Novel Stable Isotope Methods to Reconstruct Peleoenvironments: Compound-Specific Hydrogen Isotopes and Pore-Water Oxygen Isotopes. Ph. D. Thesis. Swiss Federal Institute of Technology, Zurich (141 pp).

Peterse, F., Kim, J.-H., Schouten, S., Kristensen, D.K., Koç, N., Sinninghe Damsté, J.S., 2009. Constraints on the application of the MBT/CBT palaeothermometer at high latitude environments (Svalbard, Norway). Org. Geochem. 40, 692–699.

Peterse, F., van der Meer, J., Schouten, S., Weijers, J.W.H., Fierer, N., Jackson, R.B., Kim, J.-H., Sinninghe Damsté, J.S., 2012. Revised calibration of the MBT–CBT paleotemperature proxy based on branched tetraether membrane lipids in surface soils. Geochim. Cosmochim. Acta 96, 215–229.

Pevzner, M.A., Semenenko, V.N., Vangengeim, E.A., 2003. Position of the Pontian of the Eastern Paratethys in the Magnetochronological Scale. Stratigr. Geol. Correl. 11, 482–491.

Popov, S.V., et al., 2006. Late Miocene to Pliocene palaeogeography of the Paratethys and its relation to the Mediterranean. Palaeogeogr. Palaeoclimatol. Palaeoecol. 238, 91–106.

Popov, S.V., Antipov, M.P., Zastrozhnov, A.S., Kurina, E.E., Pinchuk, T.N., 2010. Sea-level fluctuations on the northern shelf of the Eastern Paratethys in the Oligocene-Neogene. Stratigr. Geol. Correl. 18, 200–224.

Popov, S.V., Rostovtseva, Y.V., Fillippova, N.Y., Golovina, L.A., Radionova, E.P., Goncharova, I.A., Vernyhorova, Y.V., Dykan, N.I., Pinchuk, T.N., Iljina, L.B., Koromyslova, A.V., Kozyrenko, T.M., Nikolaeva, I.A., Viskova, L.A., 2016. Paleontology and stratigraphy of the middle–upper Miocene of the Taman peninsula: part 1. Description of key sections and benthic fossil groups. Paleontol. J. 50, 1–168.

Pound, Matthew J., Haywood, Alan M., Salzmann, Ulrich, Riding, James B., Lunt, Daniel J., Hunter, Stephen J., 2011. A Tortonian (Late Miocene, 11.61-7.25 Ma) global vegetation reconstruction. Palaeogeogr. Palaeoclimatol. Palaeoecol. 300, 29–45.

Prahl, F.G., Wakeham, S.G., 1987. Calibration of unsaturation patterns in long-chain ketone compositions for paleotemperature assessment. Nature 330, 367–369.

Quang, C., Liu, Y.S., Tang, H., Utesher, T., 2014. Miocene shift of European atmospheric circulation from trade wind to westerlies. Sci. Rep. 4, 5660. https://doi.org/10.1038/srep05660.

Radionova, E.P., Golovina, L.A., Filippova, N.Y., Trubikhin, V.M., Popov, S.V., Goncharova, I.A., Vernigorova, Y.V., Pinchuk, T.N., 2012. Middle-Upper Miocene stratigraphy of the Taman Peninsula, Eastern Paratethys. Central Eur. J. Geosci. 4, 188–204.

Ross, D.A., Neprochnov, Y.P., Hsü, K.J., Stoffers, P., Supko, P., Trimonis, E.S., Percival, S.F., Erickson, A.J., Degens, E.T., Hunt, J.M., Manheim, F.T., Senalp, M., Traverse, A., 1978. Initial Reports of the Deep Sea Drilling Project. vol. 42, Part 2 U.S. Government Printing Office, Washington.

Rostovtseva, Y.V., Rybkina, A.I., 2017. The Messinian event in the Paratethys: astro nomical tuning of the Black Sea Pontian. Mar. Petrol. Geol. 80, 321–332. https://doi.org/10.1016/j.marpetgeo.2016.12.005.

Roveri, M., Flecker, R., Krijgsman, W., Lofi, J., Lugli, S., Manzi, V., Sierro, F.J., Bertini, A., Camerlenghi, A., De Lange, G., Govers, R., Hilgen, F.J., Hübscher, C., Meijer, P.T., Stoica, M., 2014. The Messinian salinity crisis: past and future of a great challenge for marine sciences. Marine Geology 352, 25–58. https://doi.org/10.1016/j.margeo.2014.02.002.

Sachse, D., et al., 2004a. Reconstruction of palaeohydrological conditions in a lagoon during the 2nd Zechstein cycle through simultaneous use of dD values of individual n-alkanes and d^{18}O and d^{13}C values of carbonates. Int. J. Earth Sci. Geol. Rundsch. 93, 554–564.

Sachse, D., Radke, J., Gleixner, G., 2004b. Hydrogen isotope ratio of recent lacustrine sedimenatry n-alkanes record modern climate variability. Geochim. Cosmochim. Acta 68 (23), 4877–4889.

Sachse, D., Radke, J., Gleixner, G., 2006. dD values of individual n-alkanes from terrestrial plants along a climatic gradient - implications for the sedimentary biomarker record. Org. Geochem. 37, 469–483.

Sachse, D., Billault, I., Bowen, G.J., Chikaraishi, Y., Dawson, T.E., Feakins, S.J., Freeman, K.H., Magill, C.R., McInerney, F.A., van der Meer, M.T.J., Polissar, P., Robins, R.J., Sachs, J.P., Schmidt, H.L., Sessions, A.L., White, J.W.C., West, J.B., Kahmen, A., 2012. Molecular paleohydrology: interpreting the hydrogen-isotopic composition of lipid biomarkers from Photosynthesizing Organisms. Annu. Rev. Earth Planet. Sci. 40, 221–249.

Schimmelmann, A., Sessions, A., Mastalerz, M., 2016. Hydrogen isotopic (d/h) composition of organic matter during diagenesis and thermal maturation. Annu. Rev. Earth Planet. Sci. 34, 501–533.

Schouten, S., Hopmans, E.C., Sinninghe Damsté, J.S., 2013. The organic geochemistry of glycerol dialkyl glycerol tetraether lipids: a review. Org. Geochem. 54, 19–61.

Semenenko, V.N., 1989. Problems of the Pliocene Correlation of the East Paratethys and Tethys. Geologicky Zbornik- Geologica Carpathica, Bratislava, pp. 75–79.

Sessions, A.L., Sylva, S.P., Summons, R.E., Haynes, J.M., 2004. Isotopic exchange carbon-bound hydrogen over geologic timescales. Geochim. Cosmochim. Acta 68, 1545–1559.

Stoica, M., Lazar, I., Krijgsman, W., Vasiliev, I., Jipa, D.C., Floroiu, A., 2013. Palaeoenvironmental evolution of the east Carpathian foredeep during the late Miocene - early Pliocene (Dacian Basin; Romania). Global Planetay Change 103, 135–148.

Stoica, M., Krijgsman, W., Fortuin, A., Gliozzi, E., 2016. Paratethyan ostracods in the Spanish Lago-Mare: more evidence for interbasinal exchange at high Mediterranean Sea level. Palaeogeography, Palaeoclimatology, PalaeoecologyPalaeogeography. Palaeoclimatol. Palaeoecol. 441, 854–870. https://doi.org/10.1016/j.palaeo.2015.10.034.

Syabryaj, S., Utescher, T., Molchanoff, S., Bruch, A.A., 2007. Vegetation and palaeoclimate in the Miocene of Ukraine. Palaeogeogr. Palaeoclimatol. Palaeoecol. 253, 153–168.

Van Baak, C.G.C., Vasiliev, I., Palcu, D.V., Dekkers, M.J., Krijgsman, W., 2016. A Greigite-based magnetostratigraphic time frame for the late Miocene to recent DSDP leg 42B cores from the Black Sea. Front. Earth Sci. 4, 60. https://doi.org/10.3389/feart 2016.00060.

Van Baak, C.G.C., Krijgsman, W., Magyar, I., Sztanó, O., Golovina, L., Grothe, A., Hoyle, T., Mandic, O., Patina, I., Popov, S., Radionova, E., Stoica, M., Vasiliev, I., 2017. Paratethys response to the Messinian salinity crisis. Earth Sci. Rev. 172, 193–223.

van Dam, J.A., Abdul Aziz, H., Angeles Alvarez Sierra, M., Hilgen, F.J., van den Hoek Ostende, L.W., 2006. Long-period astronomical forcing of mammal turnover. Nature 443, 687–691.

Vasiliev, I., Krijgsman, W., Langereis, C.G., Panaiotu, C.E., Matenco, L., Bertotti, G., 2004. Towards an astrochronological framework for the eastern Paratethys Mio-Pliocene sedimentary sequences of the Focsani basin (Romania). Earth Planet. Sci. Lett. 227, 231–247.

Vasiliev, I., Iosifidi, A.G., Khramov, A.N., Krijgsman, W., Kuiper, K.F., Langereis, C.G., Popov, V.V., Stoica, M., Tomsha, V.A., Yudin, S.V., 2011. Magnetostratigraphy and radiometric dating of upper Miocene - lower Pliocene sedimentary successions of the Black Sea Basin (Taman Peninsula, Russia). Palaeogeogr. Palaeoclimatol. Palaeoecol. 310, 163–175.

Vasiliev, I., Reichart, G.J., Krijgsman, W., 2013. Impact of the Messinian Salinity Crisis on Black Sea hydrology – Insights from hydrogen isotopes on molecular biomarkers. Earth Planet. Sci. Lett. 362, 272–282.

Vasiliev, I., Reichart, G.-J., Grothe, A., Sinninghe Damsté, J.S., Krijgsman, W., Sangiorgi, F., Weijers, J.W.H., van Roij, L., 2015. Recurrent phases of drought in the upper Miocene of the Black Sea region. Palaeogeography, Palaeoclimatology, PalaeoecologyPalaeogeography. Palaeoclimatol. Palaeoecol. 423, 18–31.

Vasiliev, I., Mezger, E.M., Lugli, S., Reichart, G.J., Manzi, V., Roveri, M., 2017. How dry was the Mediterranean during the Messinian salinity crisis? Palaeoclimatol. Palaeoecol. 471, 120–133.

Volkman, J.K., Eglinton, G., Corner, E.D.S., Forsberg, T.E.V., 1980. Long chain alkenes and alkenones in the marine coccolithophorid Emiliania huxleyi. Phytochemistry 19, 2619–2622.

Weijers, J.W.H., Schouten, S., van den Donker, J.C., Hopmans, E.C., Sinninghe Damsté, J.S., 2007a. Environmental controls on bacterial tetraether membrane lipid distribution in soils. Geochim. Cosmochim. Acta 71, 703–713.

Weijers, J.W.H., Schouten, S., Sluijs, A., Brinkhuis, H., Sinninghe Damsté, J.S., 2007b. Warm arctic continents during the Palaeocene–Eocene thermal maximum. Earth Planet. Sci. Lett. 261, 230–238.

Yang, H., Pancost, R.D., Dang, X., Zhou, X., Evershed, R.P., Xiao, G., Tang, C., Gao, L., Guo, Z., Xie, S., 2014. Correlations between microbial tetraether lipids and environmental variables in Chinese soils: Optimizing the paleo-reconstructions in semi-arid and arid regions. Geochim. Cosmochim. Acta 126, 49–69.